A R C H I V E S O F M E T A L L U R G Y A N D M A T E R I A L S
Volume 54 2009 Issue 4

L. SZYMCZAK*, M. ADAMCZYK*, M. PAWEŁCZYK*

DIELECTRIC AND PYROELECTRIC PROPERTIES OF Zr – DOPED $(Ba_{0.8}Sr_{0.2})TiO_3$ CERAMICS

DIELEKTRYCZNE I PIROELEKTRYCZNE WŁAŚCIWOŚCI CERAMIK $(Ba_{0.8}Sr_{0.2})TiO_3$ DOMIESZKOWANYCH CYRKONEM

In the present paper dielectric and pyroelectric properties were investigated for ZrO_2 – doped $(Ba_{0.80}Sr_{0.20})TiO_3$ (BST 80/20) ceramics. Three dielectric peaks, corresponding to the cubic (P_C) – tetragonal (F_T), tetragonal (F_T) – orthorhombic (F_O) and orthorhombic – rhombohedral phase transitions were detected. The substitution of Ti ions by Zr ions in the B-site sublattice of BST perovskite structure causes narrowing of temperature intervals between rhombohedral-orthorhombic-tetragonal-cubic phase transitions and significant improvement of the thermostability of the pyroelectric response of BST 80/20 ceramics near room temperature.

Keywords: ceramics; barium strontium titanate; dielectric properties; pyroelectric properties; perovskite

W pracy przedstawiono rezultaty badań właściwości dielektrycznych i piroelektrycznych ceramik $(Ba_{0.80}Sr_{0.20})TiO_3$ (BST 80/20) domieszkowanych cyrkonem. W oparciu o wyniki pomiarów zależności ε'(T) stwierdzono występowanie trzech obszarów związanych z przejściami fazowymi pomiędzy fazami: paraelektryczną o symetrii układu regularnego (P_C) a ferroelektryczną fazą o symetrii układu tetragonalnego (F_T), fazą tetragonalną (F_T) a ferroelektryczną fazą o symetrii układu rombowego (F_O) oraz fazą rombową a ferroelektryczną fazą o symetrii układu romboedrycznego (F_R). Podstawienie jonów Zr w podsieć B wyjściowego związku powoduje zanik fazy rombowej i tetragonalnej na rzecz poszerzenia temperaturowego zakresu występowania fazy romboedrycznej. Powoduje to, iż w zakresie temperatur bliskich temperaturze pokojowej, zwiększa się termiczna stabilność piroelektrycznej odpowiedzi, badanych ceramik, na zmianę temperatury.

1. Introduction

High performance and low-cost infrared (IR) sensors are required for thermal detection and imaging objects at or near the ambient temperature. Pyroelectric IR sensors are promising more convenient sensing system because of a high sensitivity at a long-wavelength and room temperature operation without cooling systems [1-5].

(Ba,Sr)TiO_3 (BST) has large values of the relative dielectric permittivity and the spontaneous polarization with relatively small values of the dielectric losses. Moreover, its Curie temperature (T_C) can be suitably controlled by adjustment the ratio of Ba to Sr [6-8]. In the light of this, BST has been extensively studied as a prime candidate material for thermal imaging sensors, DRAM devices and multi-layer ceramic capacitors. On the other hand, BST exhibits a strong temperature dependence of the pyroelectric coefficient, which is detrimental to the reliability of IR sensing characteristics. To improve the thermostability of pyroelectric response, it is necessary to look for a composition characterised by the ferroelectric – paraelectric transition occurring continuously over a broad temperature range.

In the present paper we report the result of experimental study concerning influence of ZrO_2 dopant on the phase transitions, dielectric and pyroelectric properties of $(Ba_{0.8}Sr_{0.2})TiO_3$ ceramics.

2. Experimental details

The BST ceramics of the composition 80/20 pure and doped by 1-10 mol% ZrO_2 were prepared using the conventional mixed-oxide processing technique. Stoichiometric amounts of $BaCO_3$, $SrCO_3$ and TiO_2 oxides, together with the target amount of ZrO_2 additive were weighed and mixed. Thermal synthesis of mixed and pressed oxides was carried out at T_S = 925°C for t_S=4h. Crumbled, milled and sieved materials were pressed again in the form of cylinders and then sintered at T_S=1250°C for t_S=4h. This procedure was repeated

* INSTITUTE OF PHYSICS, UNIVERSITY OF SILESIA, 40-007 KATOWICE, UNIWERSYTECKA 4, POLAND

again before the final sintering at T_S=1460°C for t_S=7h. The obtained ceramics with 91-95% theoretical density had good mechanical quality.

The scanning electron microscope (SEM), JSM-5410 with an energy dispersive X-ray spectrometer (EDS) with Si(Li) X-ray detector was used for investigating structure and composition of the obtained ceramics. The grain size measurements were performed on fracture surface of the ceramics.

The X-ray diffraction measurements (XRD) were carried out at room temperature on all ceramic samples using Huber diffractometer (Seemann-Bohlin geometry) with monochromatic Cu-Kα_1 radiation (30kV, 30mA). The angle scale of received diffraction diagrams was scaled to 2θ (Bragg-Brentano geometry) by Au standard (JCPDS number 12-0403). The diagrams were measured from 20 to 100° in 2θ with 0.05° steps. The calculations were performed using the software for treatment of powder X-ray diffraction data DHN_PDS. In order to receive exact locations, intensities and widths of diffraction lines, the experimental data were fitted to theoretical functions. The attempts of fitting by Gaussian (G), Lorenzian (L), modified Lorenzian (ML) and intermediate Lorenzian (IL) were made. The IL profile showed the best agreement with experimental data and this profile was taken to fit all segments of diagram including diffraction lines. The data received in this manner were used to calculate the unit cell parameters.

An automatic measuring system with HP4192A impedance analyzer was used to measure and record the temperature dependencies of the dielectric constant (ε') and the loss factor (tan δ) at frequencies 0.1kHz – 100kHz of the measuring field. The characteristics ε'(T) and tan δ(T) were obtained in successive heating-cooling cycles with a constant rate of 2.5°C/min.

The temperature dependence of remanent polarization (P_r) was determined from the hysteresis loop measurements in the field of frequency 50Hz and strength 10kV/cm.

The pyroelectric effect was measured for mechanically free samples using the quasi- static method, i.e. by recording the pyroelectric current during linear temperature changes. Prior to each measurement the samples were first polarised in dc electric field of strength 3 kV/cm applied for 10 min at temperature T_p = 100°C and then cooled in the field to –50°C at which the field was switched off. The samples were then heated with constant rate of 5°C/min. through all three phase transitions to the temperature 450°C. The pyroelectric current and the thermally stimulated depolarisation current (TSDC) were recorded numerically as a function of temperature and time during heating.

3. Results and discussion

3.1. SEM study

Images of the grain structure on the fracture surface of BST 80/20 ceramics with ZrO_2 content 1 and 10 mol% are shown in Fig. 1, as an example. The grain sizes were in range of 4 ÷ 20 μm and 2 ÷ 6 μm for the ceramics with 1 and 10 mol% of ZrO_2, respectively. The average grain size of undoped ceramics was larger than 30μm [9]. The ZrO_2 addition produces slightly smaller grains with increasing concentration. The decrease in grain size with increasing Zr content can be associated with the lower grain-growth rate caused by slow diffusion of the larger Zr^{4+} ion in place of smaller Ti^{4+} ion. The grain size reduction also implies that the crystallization of BSZT becomes more difficult as a result of Zr incorporation [10].

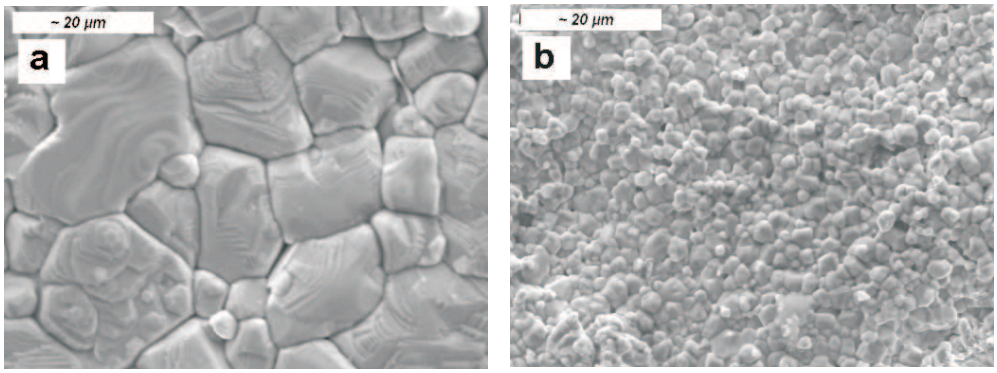

Fig. 1. SEM images of the fracture surface of BST 80/20 + 1 mol% ZrO_2 (a) and BST 80/20 + 10 mol% ZrO_2 (b) ceramics

The EDS analysis indicated a homogeneous distribution of all the elements throughout the grains.

3.2. X-ray measurements

XRD patterns show that the crystal structures exhibit tetragonal symmetry at room temperature for undoped and containing 1 – 5 mol% ZrO_2 BST 80/20 ceramics. When ZrO_2 content is larger than 5 mol% (7 and 10 mol% of ZrO_2) the crystal structure exhibits rhombohedral symmetry at room temperature.

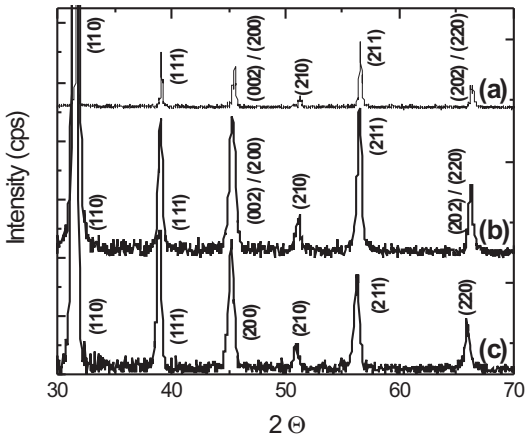

Fig. 2. Parts of the diffraction patterns obtained at the room temperature for undoped BST 80/20 ceramics (a) and doped 1 mol% (b) and 10 mol% (c) ZrO_2

In all of them a single phase, isostructural perovskite solid solutions, is observed. The example of X-ray diffraction patterns of undoped BST 80/20 ceramics and with 1 and 10 mol% ZrO_2 content obtained at room temperature is shown in Fig. 2 Unit cell parameters were calculated for all doped BST 80/20 ceramics which allowed to determine the average unite cell parameter $\overline{a} = V^{1/3}$ (where V is a unit cell volume). The dependence $\overline{a}$ versus ZrO_2 concentration is presented in Fig. 3. One can notice that the unit cell volume increases with an increase in dopant concentration which seems to confirm the supposition that Ti^{4+} ions in solid solutions are substituted by Zr^{4+} ions with larger ionic radius.

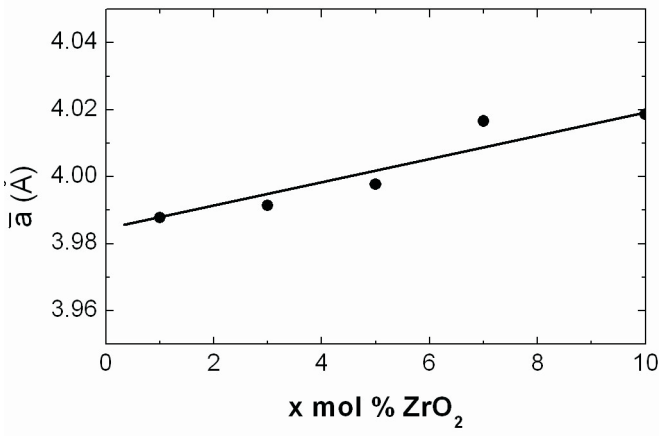

Fig. 3. Average cell parameter versus ZrO_2 content for BST 80/20 ceramics

3.3. Dielectric properties and phase transitions diagram

Some characteristics ε'(T) and tan δ(T) obtained on heating at the measuring field of frequency 1kHz, for undoped and Zr-modified BST 80/20 ceramics are shown in Fig. 4. It can be seen that for ZrO_2 content smaller than 5 mol%, both ε'(T) tan δ(T) curves reveal anomalies in the vicinity of temperatures corresponding to the orthorhombic-tetragonal (F_O-F_T) and tetragonal-cubic (F_T-P_C) phase transitions (Fig. 4). An anomaly in the vicinity of temperatures corresponding to the rhombohedral-orthorhombic (F_R-F_O) phase transition, for ceramic with 5 mol% ZrO_2, is visible only in dε'/dT (T) dependence. The temperature intervals between the three phase transitions become narrower when Zr concentration increases. The three anomalies in ε'(T) curves associated with the structural phase transitions

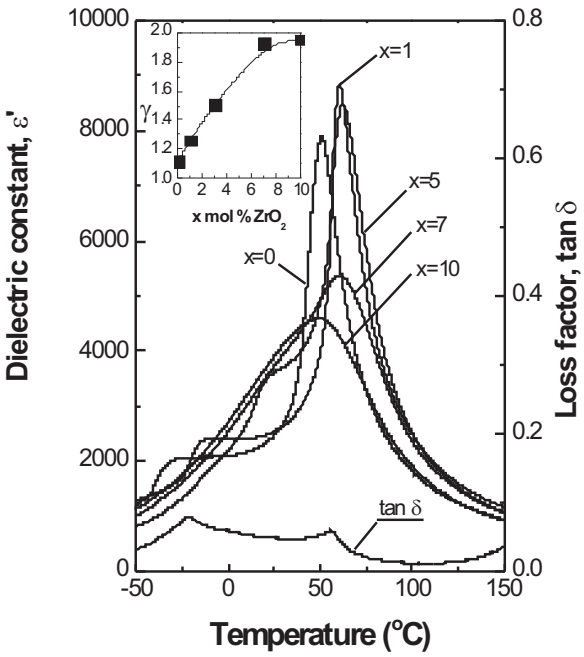

Fig. 4. Dielectric constant as a function of temperature, measured on heating at frequency of measuring field 1kHz for BST 80/20 + x mol% ZrO_2 ceramics. Diffuseness exponent γ vs. ZrO_2 content is shown in the inserted figure. The example of loss factor vs. temperature, measured for ceramics doped 1 mol% ZrO_2, is also shown in the Figure

eventually merge into a broad peak for the largest zirconium concentrations, i.e. 7 and 10 mol% (Fig. 4). Based on the dielectric measurements, the phase transitions temperatures diagram of BST 80/20 + x mol% ZrO_2 ceramics was plotted (Fig. 5). The $T_{F_R-F_O}$ phase transition temperature for undoped BST 80/20 ceramics shown in this figure is quoted according to [7].

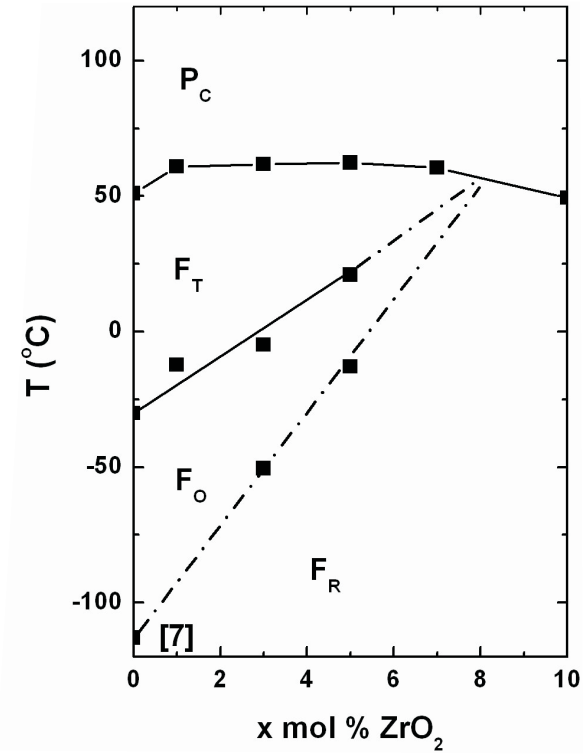

Fig. 5. Variations of phase transitions temperatures versus ZrO_2 content

The ε'(T) curves presented for all investigated ceramics show a strongly diffuse character of ferroelectric-paraelectric phase transition (DPT). Diffusion increases with an increase in the ZrO_2 content. The quantitative assessment of the diffusion (γ) in the paraelectric phase was evaluated using the formula:

$$1/\varepsilon' - 1/\varepsilon'_{max} = C(T - T_m)^{\gamma} \qquad (1)$$

where temperature $T_m \equiv T_{F_T-P_C}$ corresponding to maximum value of dielectric constant ε'_{max}. The determined coefficient γ versus Zr content is also shown in Fig. 4. It can be noted that the value of exponent γ depends strongly on the ZrO_2 content. The Curie-Weiss law (γ=1) was observed only at temperatures much higher than T_m.

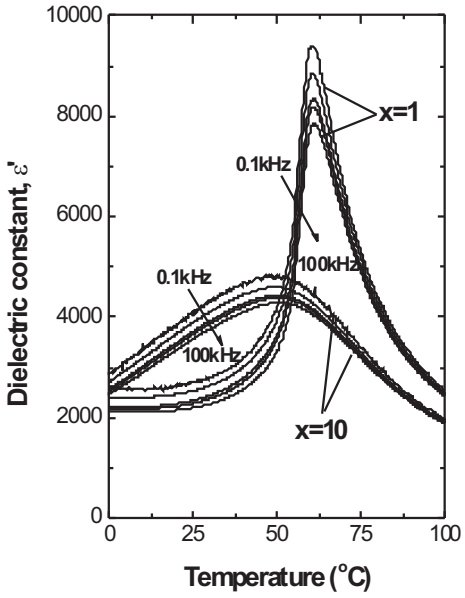

Fig. 6. The temperature dependence of ε' for BST 80/20 + x mol% ZrO_2 ceramics for various frequencies of measuring field

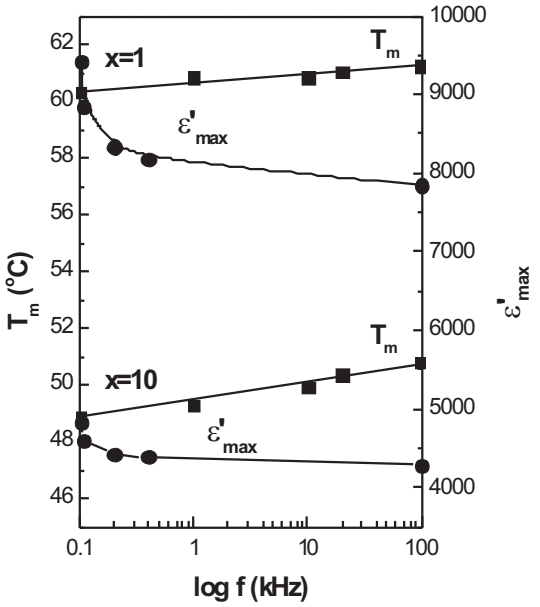

Fig. 7. The maxima in ε'(T) curves and corresponding temperatures T_m as a function of frequency of measuring field for BST 80/20 ceramics with various ZrO_2 content

The characteristics ε'(T) for various frequencies of the measuring field are shown in Fig. 6 for the ceramics with 1 and 10 mol% of ZrO_2. The ε_{max} is strongly dependent on the frequency of the electric field applied to both these ceramics (Fig. 6 and Fig. 7), whereas the temperatures T_m corresponding to these maxima are weakly dependent on the frequency (Fig. 7). The frequency dependence of ε'_{max} is relatively more distinct for the BST 80/20 ceramics doped with 1 mol% of ZrO_2.

All investigated ceramics show additional anomalies in ε'(T) and tan δ(T) characteristics in the range of the cubic paraelectric phase apart from the above shown anomalies in the surroundings of $F_O - F_T$ and $F_T - P_C$ phase transitions. These additional anomalies and their low frequency dispersion are shown in Figs. 8(a) and 8(b) for 1 and 10 mol% ZrO_2-modified BST 80/20 ceramics, respectively. Such behaviour was found for many

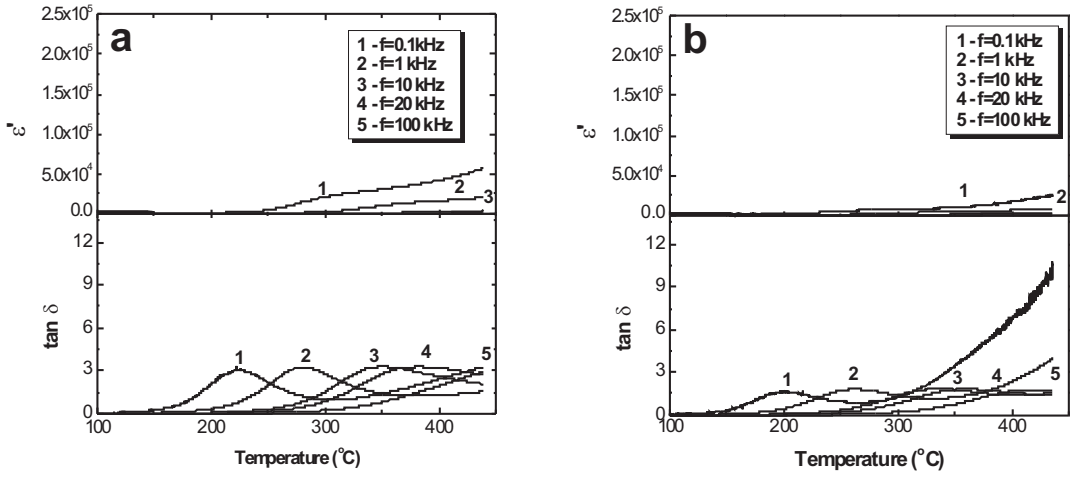

Fig. 8. Temperature dependence of ε' and tan δ measured in the range of paraelectric phase at frequencies from 0.1kHz to 100kHz for BST 80/20 + 1 mol% ZrO_2 (a) and BST 80/20 + 10 mol% ZrO_2 (b)

ferroelectrics with the perovskite-type structure [11,12], as well as for undoped BST 80/20 ceramics [9]. The observed anomalies in ε'(T) and tan δ(T) characteristics origin from occurrence of polar micro regions, associated with non-homogeneous distribution of ion defects. These polar micro regions are the traces of non-randomly distributed space charges, previously participating in the screening of ferroelectric domains [13]. The insertion of the Zr dopant to ceramics caused gradual decay of this dispersion in the region of the paraelectric phase.

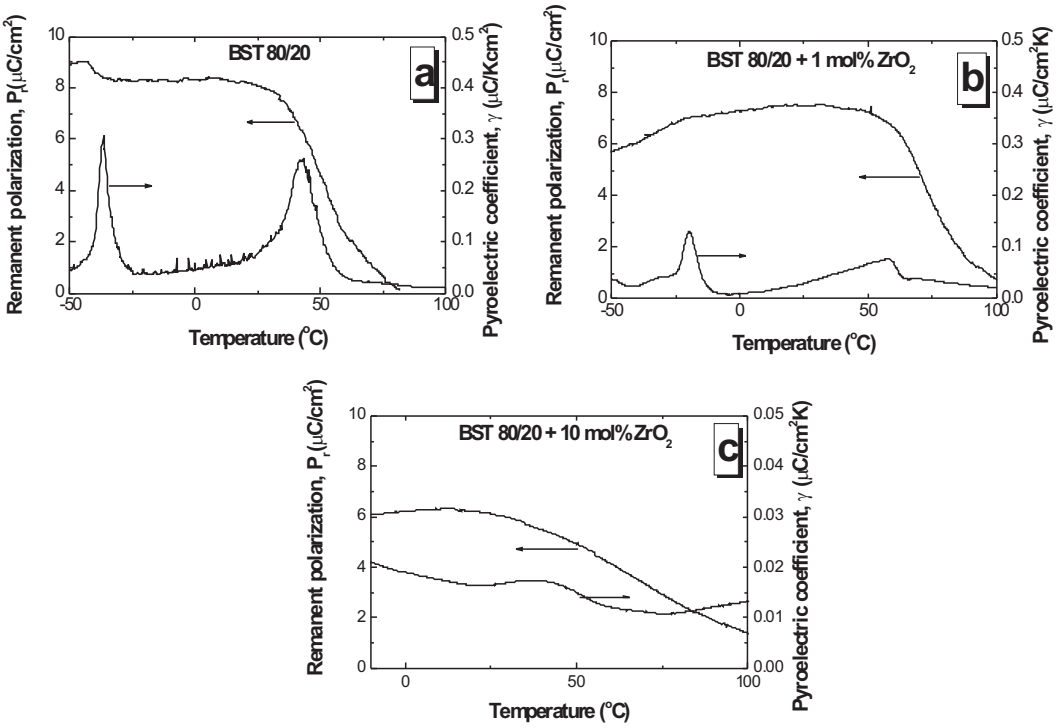

Fig. 9. The pyroelectric coefficient and remanent polarization versus temperature for BST 80/20 ceramics with various ZrO_2 content

The temperature dependences of the remanent polarization (P_r) obtained on heating for BST 80/20 ceramics with various ZrO_2 contents, are shown in Fig. 9. The course of the P_r(T) curves differ markedly from that observed in the normal ferroelectrics with first order ferroelectric-paraelectric phase transition particularly, in a wide temperature range in the neighborhood of T_m (Fig. 9). In the case of undoped BST ceramics the maximum value of P_r is small ($P_r \approx 8\mu C/cm^2$) at room temperature and gradually decreases with zirconium concentration to ca. $6\mu C/cm^2$ for x = 10 mol% ZrO_2.

3.4. Pyroelectric and thermally stimulated depolarization currents

The measurements of pyroelectric and thermally stimulated depolarization currents (TSDC) were carried out for better understanding the behaviour of dielectric characteristics, shown above.

The dependence of a pyroelectric coefficient γ vs temperature, obtained for the ceramics with various contents of ZrO_2 is shown in Fig. 9. It can be seen that for the undoped (Fig. 9(a)) and Zr (1 mol%) doped (Fig. 9(b)) ceramics, the γ(T) curves show characteristic peaks at temperatures, which can be identified with the $F_O - F_T$ and $F_T - P_C$ phase transitions temperatures. Therefore, the temperature intervals between the observed phase transitions become narrower as Zr ions are substituted for Ti ions in the B-site sublattice of the perovskite structure. The three peaks associated with the structural phase transitions eventually coalesce together, exhibiting a broad pyroelectric response at higher Zr concentrations (Fig. 9(c)).

As it was mentioned above, the studied BST ceramics demonstrate low frequency dispersion at high temperatures of the paraelectric phase (Fig. 6). This additional dispersion originates from the non-homogeneous distribution of ion space charges participating in the screening process of the polar-regions [14]. The occurrence of the polar micro regions and their interaction with free electron and ion space charges can be also identified by thermally stimulated depolarization current studies. The temperature changes of the observed TSDC, for undoped and Zr-modified BST 80/20 ceramics are shown in Fig. 10. The TSDC with broadened maximum appeared at

temperatures higher than the temperature at which the ceramics were pre-polarized. When the content of zirconium increased the termal depolarization current decreased.

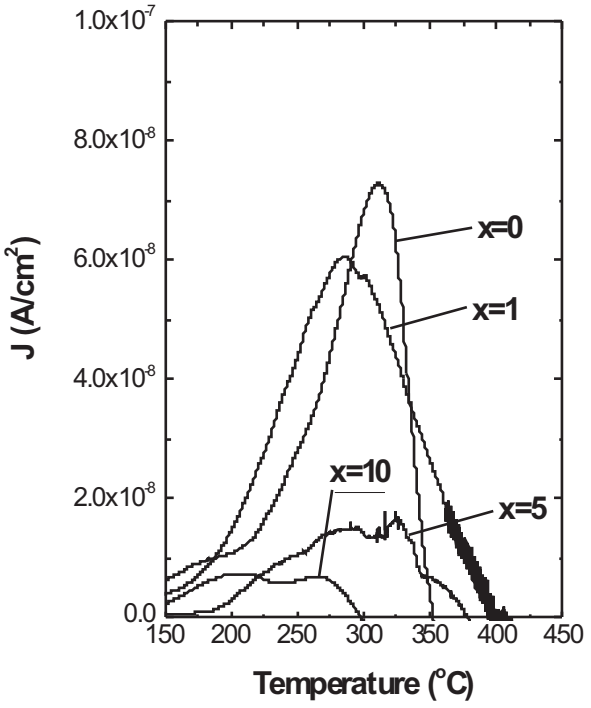

Fig. 10. Thermally stimulated depolarization currents as a function of temperature for BST 80/20 + x mol% ZrO_2 ceramics, pre-polarized at constant temperature (Tp=100°C) in a dc field of 3 kV/cm during 10 min

4. Conclusions

The obtained experimental data show that the Zr dopant strongly influences on all the investigated characteristics of BST 80/20 ceramics. The increase of the Zr concentration leads to the decrease of grain size, the increase of density and the improvement of the quality of the investigated ceramics. The temperature intervals between the three consecutive ferroelectric transitions become narrower as Zr^{4+} ions are substituted for Ti^{4+} ions in the B-site sublattice of BST 80/20 ceramics and as the results of this, three peaks associated with the structural phase transitions coalesce, exhibiting a broad dielectric response for ZrO_2 content higher than 5 mol%. Additional anomalies in ε'(T) and tan δ(T) curves in the low frequency range, present in the paraelectric phase for the undoped ceramics, are eliminated by the Zr dopant.

REFERENCES

[1] S. T. Liu, D. Long, Pyroelectric detectors and materials, device and applications Proc.IEEE **66**, 14 (1978).

[2] R. Watton, Ferroelectric materials and devices in infrared detection and imaging Ferroelectrics **91**, 87 (1989).

[3] R. W. Whatmore, A. Patel, N. M. Shorrocks, F. W. Ainger, Ferroelectric Materials for Thermal IR Sensors State-Of-The-Art And Perspectives Ferroelectrics **104**, 269 (1990).

[4] R. W. Whatmore, Pyroelectric Ceramics and Devices for. Thermal Infra-red Detection and Imaing Ferroelectrics **118**, 241 (1991).

[5] R. Watton, M. A. Todd, Induced pyroelectricity in sputered lead scsndium tantalate films and their merit for IR detector arrays Ferroelectrics **118**, 279 (1991).

[6] U. Syamaprasad, R. K. Galgali, B. C. Mohanty, Dielectric properties of the $Ba_{1-x}Sr_xTiO_3$ system Mater.Lett. **7**, 197 (1988).

[7] V. V. Lemanov, E. P. Smirnova, P. P. Syrnikov, E. A. Tarakanov, Phase transitions and glasslike behaviour in $Sr_{1-x}Ba_xTiO_3$ Phys.Rev. **B 54**, 3151 (1996).

[8] R. Wang, Y. Inaguma, M. Itoh, Dielectric properties and phase transition mechanisms in $Sr_{1-x}Ba_xTiO_{rm3}$ solid solution at low doping concentration Mater.Res.Bull. **36**, 1693 (2001).

[9] L. Szymczak, Z. Ujma, J. Hańderek, J. Kapusta, Sintering effects on dielectric properties of (Ba,Sr)TiO_3 ceramics Ceramics International **30**, 1003-1008 (2004).

[10] I. Chyuan, S. L. Fu, Effects of zirconium on the structural and dielectric properties of (Ba,Sr)TiO_3 solid solution, J. Mater. Sci. **25**, 4699 (1990).

[11] Z. Ujma, L. Szymczak, J. Hańderek, K. Szot, H. J. Penkalla, Dielectric and pyroelectric properties of Nb-doped $Pb(Zr_{0.92}Ti_{0.08})_{O3}$ ceramics J. Eur. Ceram. Soc. **20**, 1003-1010 (2000).

[12] M. Maglione, Dielectric relaxation and conductivity in ferroelectric perovskites Ferroelectrics **176**, 1-6 (1996).

[13] J. Hańderek, Z. Ujma, C. Carabatos-Nedelec, G. Kugel, D. Dmytrów, I. El-Harrad, Dielectric, pyroelectric, and thermally stimulated depolarization current investigations on lead-lanthanum zirconate-titanate-x/95/5 ceramics with La content x=0.5%-4% J. Appl. Phys. **73**, 367-373 (1993).

[14] D. Viehland, S. Jang, L. E. Cross, M. Wutting, J.Appl. Phys. **68**, 2916 (1990).

Received: 10 September 2009.